African Journal of Biological Sciences

https://doi.org/ 10.33472/AFJBS.6.5.2024. 3725-3739

Green synthesis of Cu doped zinc oxide nano antibiotic: characterization and effect of Cu doping on antibacterial activity

Goutam Mandal[1] and Baibaswata Bhattacharjee[2*]

[1]Department of Physics, Bankura Zilla Saradamani Mahila Mahavidyapith, Bankura-722101, West Bengal, India,
[1]Department of Physics, Bankura University, Bankura-722146, West Bengal, India.
[2]Department of Physics, Ramananda College, Bishnupur, Bankura-722122, W.B., India.
[*]Corresponding author (*): Ramananda College, Bishnupur, Bankura, West Bengal, India, 722122; Email: baib23@gmail.com; Tel.: (+91)8250683692

Article History
Volume 6, Issue 5, 2024
Received: 09 May 2024
Accepted: 17 May 2024
doi: *10.33472/AFJBS.6.5.2024. 3725-3739*

Abstract

This study synthesized $Zn_{1-x}Cu_xO$ nanoparticles (x=0.0, 0.02, and 0.04) from *Calotropis gigantea* leaf extract utilizing green synthesis. The effect of Copper (Cu) doping on optical properties, structure, and morphology were examined using XRD, SEM, and UV-Vis spectroscopy. XRD confirmed hexagonal wurtzite unit cell. As Cu concentrations increased, nanoparticle micro-strain and dislocation density decreased while bond length, crystallite size, lattice constant, and unit cell volume increased. The atomic packing percentage was 73.12%, and the bond length ranged from 1.988 to 1.990 Å. FESEM revealed spherical nanoparticles. Doping red-shifts the band gap (E_g) of nanoparticles from 3.31 to 3.02 eV. The green synthesized $Zn_{1-x}Cu_xO$ nanoparticles are used for the first time as a nano antibiotic. The $Zn_{1-x}Cu_xO$ nanoparticles were tested for antibacterial activity against gram-positive (*S. pyogenes*) and gram-negative (*E. coli*) using the agar well diffusion method. The antibacterial results demonstrated that Cu-doped ZnO NPs had a larger inhibitory zone diameter throughout the chosen bacteria.

Keywords

Calotropis gigantea, Cu doped ZnO, Structural analysis, Optical analysis, Bacteria, Antibacterial activity.

1. Introduction

Nowadays, bacterial infection poses a severe and substantial hazard to human life worldwide. Furthermore, the synthesized antibiotic has comparable biocompatibility, ensuring its safe use in clinical applications (Ali et al., 2020). Healthcare-associated infection (HCAI), sometimes referred to as nosocomial infection, affects a substantial number of patients and continues to be a primary source of occupational infection among facility workers. It creates a significant financial burden on healthcare services and is associated with increased patient illness and death rates (Donlan, 2008). The World Health Organization (2016) reports that healthcare-associated infections (HCAIs) are responsible for around 56% of neonatal fatalities. In South-East Asia and Sub-Saharan Africa, the prevalence rate of HCAIs is as high as 75% (Okeke et al., 2020). Chemical-based disinfectants have been linked to higher rates of HCAI, drug-resistant bacteria, toxicity, and carcinogenicity, raising severe concerns. Therefore, it is necessary to create alternative methods for developing a more advanced antibacterial substance using inorganic minerals to reduce the impact of healthcare-associated infections (HCAIs).

Recently, there has been a significant focus on synthesizing metal and metal oxides (MO) due to their potential bactericidal and bacteriostatic uses in nanomedicine. Compared to other MO, Zinc oxide nanoparticles (ZnO NPs) stand out with their large exciton binding energy of 60 meV and broad direct band gap of 3.37 eV (Wijesinghe et al., 2021). Because of its non-toxicity, strong catalytic activity, and economy, ZnO NPs have gained recognition as an alternative photocatalyst (Majumder et al., 2021). Additionally, it possesses excellent thermal stability, electrochemical properties, and visible-light transparencies (Hezam et al., 2018). ZnO NPs are highly regarded as advanced materials for their biocidal and disinfecting properties. Prototype ZnO nanoparticles (NPs) have been utilized as delivery systems for vaccines and anticancer drugs, showcasing their potential in the field (Jhaveri et al., 2021).

Furthermore, significant research has been dedicated to modifying the band structure of ZnO to enable its responsiveness to visible light (Zhang et al., 2021). A highly successful method is doping, which creates new electronic states inside ZnO's band gap energy, providing additional paths for electronic transition and red-shifting the absorption band to the visible range (Samadi et al., 2016). Transition metals like copper are extensively used to dope ZnO particles to boost visible light absorption and photocatalytic activity by prolonging UV Vis. absorption, generating surface oxygen vacancies, and limiting charge carrier recombination (Gaurav et al., 2019). Superior photocatalytic and antibacterial properties were observed in

Cu-doped ZnO nanorods compared to pure ZnO nanorods (Shanmugam and Jeyaperumal, 2018).

Many physical and chemical approaches synthesize ZnO NPs with different physical and morphological properties (Mintcheva et al., 2018; Devi and Velu, 2016; Al Abdullah et al., 2017; Navidpour et al., 2023; Jain et al., 2009). However, hazardous ingredients, high temperature and pressure, high cost, and long-time requirements have led research to focus on clean and eco-friendly synthesis techniques (Salem and Fouda, 2021). Recently, simple and economical green processes make metal and metal oxide nanoparticles from plants, plant extracts, and microorganisms. Green synthesis using plants and plant extracts was preferred over other microbes because of its simplicity, large-scale facilitation, and safe, non-toxic production (Mohamad et al., 2014).

Natural reducing and capping agents include plant components and extracts (Berehu et al., 2021). Green ZnO-NP synthesis has garnered researchers' attention, and numerous organizations are working on it. Synthesis of ZnO NPs has been reported from several plants and leaf extracts (Ahmed ET AL., 2017).

One member of the Asclepiadaceae family, *Calotropis gigantea,* is most often known as milkweed (Karale et al., 2017). Geographically, the plant is widespread over India, but it is most common on Andaman Island, where it may be found on hills up to an elevation of 900 meters. Traditional medicine has long made use of *Calotropis gigantea (L.)* Dryand alleviates bronchitis, asthma, leprosy, dermatitis, and elephantiasis symptoms.

In light of the preceding, we detail the structural, optical, and morphological characteristics of undoped and Cu-doped ZnO NPs synthesized by an efficient and environmentally friendly method utilizing *C. gigantea (L.).* The agar well diffusion method was also used to assess the antibacterial activity of the produced Cu-doped ZnO NPs against clinical isolates of gram-positive (*Streptococcus pyogenes*) and gram-negative (*Escherichia coli*) bacteria.

2. Materials and Methods

2.1. Materials

The chemicals zinc acetate dihydrate [$Zn(CH_3CO_2)_3.2H_2O$], copper(II) acetate [$Cu(CO_2CH_3)_2$], and sodium hydroxide [NaOH] were purchased from Sigma Aldrich, hydrochloric acid [HCl] was purchased from Loba Chemical and used as obtained. On the other hand, nutrient agar (NA) was purchased from Hi-media Pvt. Ltd. All chemicals were of analytical reagent grade, and double distilled water was used to prepare all solutions.

2.2. Collection of *C. gigantea*

C. gigantea leaves were gathered in the district of Bankura (23.1645° N, 87.0624° E), West Bengal, India. The leaves were thoroughly washed in tap water before being cleaned with distilled water and cut with a clean knife. The leaves were dried in a hot oven at 60°C for 8 hours, and the powdered leaves were stored at room temperature in an airtight container until use.

2.3. Preparation of leaf extract

To make leaf extract, 6 g of dried leaf powder was added to 100 ml of distilled water and boiled at 60^0 C for 15 minutes. The solution was allowed to cool to room temperature before being filtered using filter paper. The filtrate was collected in an amber container and kept in a deep freezer for future investigations.

2.4. Green synthesis of undoped and Cu doped ZnO nano antibiotic

The nanoantibiotic was produced at room temperature using a noble green synthesis technique. Initially, 2.195 g of zinc acetate dihydrate was dissolved in 50 mL of distilled water to prepare a 0.2 M solution. The stoichiometric quantity of copper acetate was estimated using $Zn_{1-x}Cu_xO$ (where x = 0.0, 0.02, and 0.04) and mixed with zinc acetate dihydrate while stirring continuously. After 15 minutes, 20 mL of *C. gigantea* leaf extract and 30 mL of 1M NaOH were added dropwise to make a 100 mL solution. Stirring was continued for up to 3 hours, after which the solution was allowed at room temperature to precipitate. The residue was dried in an incubator at 50^0 C before ground into a fine powder using a ceramic pestle and mortar. The powder was ultimately calcined at 250^0 C for 4 hours. The schematic synthesis process is depicted in Figure 1.

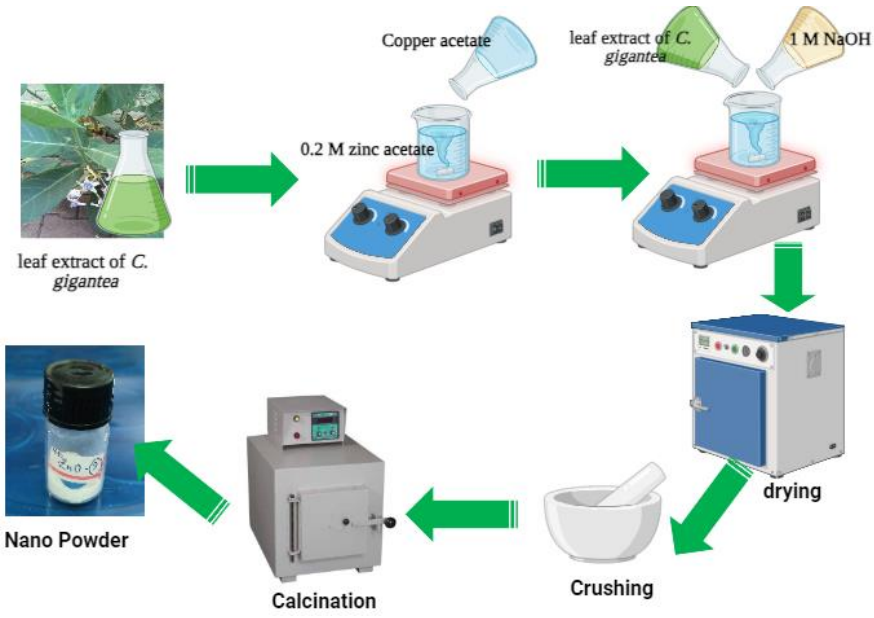

Figure 1. Schematic diagram of the synthesis of $Zn_{1-x}Cu_xO$ nano antibiotics

2.5. Characterization tools

X-ray diffraction (XRD) data were acquired in a Rigaku X-ray diffractometer using Cu-Kα radiation with a wavelength of 1.54 Å over an angular selection of 20° to 80°. A Systronics AU 2703 double-beam UV-Vis. spectrophotometer with a wavelength range of 200 to 800 nm was used for optical absorption measurements. A ZEISS field emission scanning electron microscope (FESEM) was used to analyze the surface morphology of the catalysts at accelerating voltages of 5 kV.

2.6. Screening of antibacterial activity of $Zn_xCu_{1-x}O$ NPs

To test the antibacterial activity of Cu-doped ZnO NPs, all bacterial strains were sub-cultured from pure cultures in Mueller-Hinton broth medium and incubated overnight at 37˚C. The turbidity of the bacterial culture is adjusted to the newly manufactured 0.5 McFarland turbidity standard, corresponding to (1.5×10^8 CFU/mL) bacteria (Wiegand et al., 2008). Approximately 25 ml of prepared nutrient agar was planted in a sterile plate alongside 24 h bacterial cultures by dipping a sterile cotton swab into the broth of these microorganisms. The plates were let to stand for around 10 to 15 minutes to allow the culture to permeate into the media. Each bacterial species is aseptically swabbed onto a separate Muller-Hinton agar plate using sterile cotton swabs. After solidification, a sterile cork borer made 6 mm bores in each petri plate. Then, 0.1 mL (100 µg/mL) of each NP (undoped and doped ZnO) dissolved in 2% Hydrochloric acid (HCl) was poured into the wells and incubated for 24 hours at 37°C. All plates are incubated overnight at 37˚C. The control test consisted of HCl alone, without any NPs. After incubation, the diameter of inhibition zones (mm) was measured to determine the antibacterial activity of the samples.

The zone of inhibition (ZOI) around each well was measured in millimeters using calipers. Clindamycin phosphate (20 µg/mL) serves as the standard reference antibiotic.

3. Results and discussion

3.1. Optical properties

The optical absorption spectroscopy of undoped and Cu-doped ZnO nanoparticles (NPs) was examined using UV-visible absorption spectroscopy at ambient temperature. Figure 2(A) displays the UV Vis absorption spectra of the produced nanoparticles. Figure 2(A)

demonstrates a prominent excitonic absorption peak at 385 nm, 383 nm, and 378 nm for ZnO, $Zn_{0.98}Cu_{0.02}O$, and $Zn_{0.96}Cu_{0.04}O$, respectively. The presence of these peaks can be attributed to the high exciton binding energy and excellent optical quality of the produced nanoparticles. Furthermore, the peaks seen in all samples exhibit a blue shift compared to bulk ZnO. Figure 2(A) demonstrates that all Cu-doped NPs exhibit superior absorption of visible light compared to undoped NPs. The band gap has been further computed using The Tauc equation (Tauc et al., 1966) was utilized to calculate the optical band gap (E_g) of the nanoparticles, as follows:

$$(\alpha h\upsilon)^n = B(h\upsilon - E_g) \quad (1)$$

The variables in question are as follows: α represents the absorption coefficient, h represents Planck's constant, υ represents frequency, and B represents the band tailing parameter. The value n is determined by the kind of transition, with possible values of 1/2, 2, 3/2, and 3 corresponding to allowed direct, allowed indirect, forbidden direct, and forbidden indirect transitions, respectively (Guneri et al., 2010). Zinc oxide (ZnO) is classified as a direct band gap material, which means that the value of the band gap exponent (n) is considered to be 1/2.

The band gap energy was determined by analyzing the linear portion of the graph of $(\alpha h\upsilon)^2$ vs. hυ (Figure 2(B)). The precise band gap values found are 3.31 eV, 3.18 eV, and 3.02 eV for ZnO, $Zn_{0.98}Cu_{0.02}O$, and $Zn_{0.96}Cu_{0.04}O$, respectively. An observation has been made that the band gap of doped ZnO nanoparticles reduces with an increase in the concentration of Cu doping. Furthermore, the reduction in band gap might be attributable to integrating an impurity band with a conduction band (Bylsma et al., 1986). Therefore, the red shift in the Cu-doped samples proves that Cu has been uniformly integrated into the ZnO lattice.

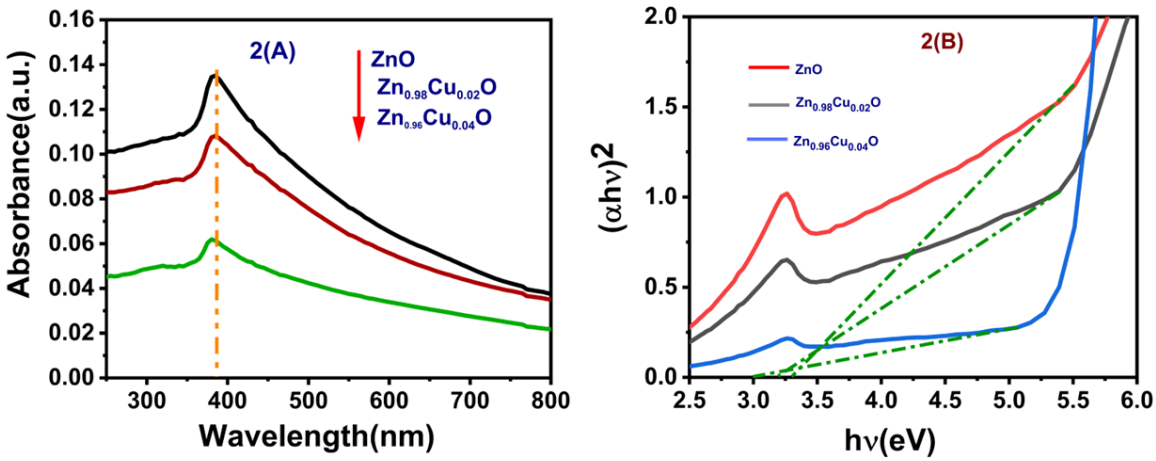

Figure 2. (A) UV absorption spectra of undoped and Cu-doped ZnO nano antibiotic (B) Touc plot of undoped and Cu-doped ZnO nano antibiotic.

3.2. Structural analysis

3.2.1. FESEM

The FESEM was employed to analyze the impact of different concentrations of Cu on the particle length and surface morphology of ZnO NPs. The FESEM analysis of ZnO NPs was studied to investigate the surface morphology, size, shape, and growth mechanism. The micrograph of all the samples is displayed in Figure 3(A, B, and C). The FESEM image displays nearly spherical and randomly oriented nanoparticles. The Cu sites can be seen in the pictures.

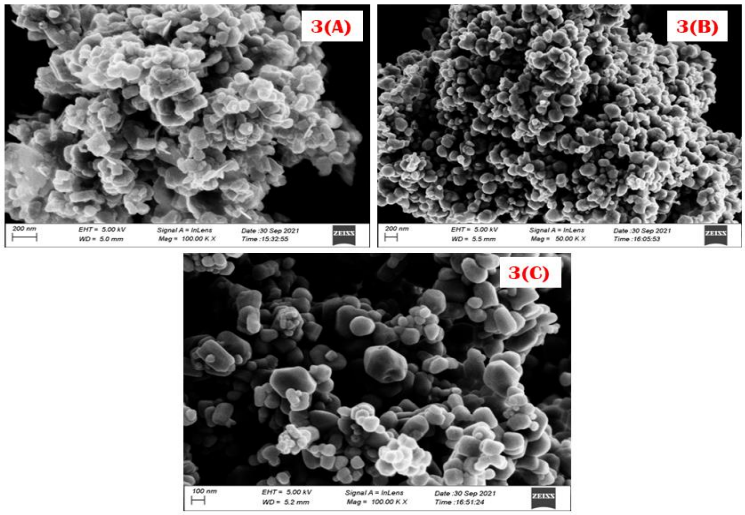

Figure 3. (A) SEM micrograph of ZnO NPs (B) SEM micrograph of $Zn_{0.98}Cu_{0.02}O$ NPs (C) SEM micrograph of $Zn_{0.96}Cu_{0.04}O$ NPs

3.2.2. XRD Spectra

The XRD pattern of all the nanocrystals is shown in Figure 4. It shows that the unit cell of the synthesized ZnO nanocrystals is hexagonal with the presence of the peaks (100), (002), (101), (102), (110), (103), (200), (112), and (201). The planes are randomly oriented (Liang et al, 2009) and can be well indexed to the hexagonal (wurtzite) phase of crystalline ZnO matched with JCPDS file no. 96-210-7060. The XRD peak positions of all the samples are shown in Table 1.

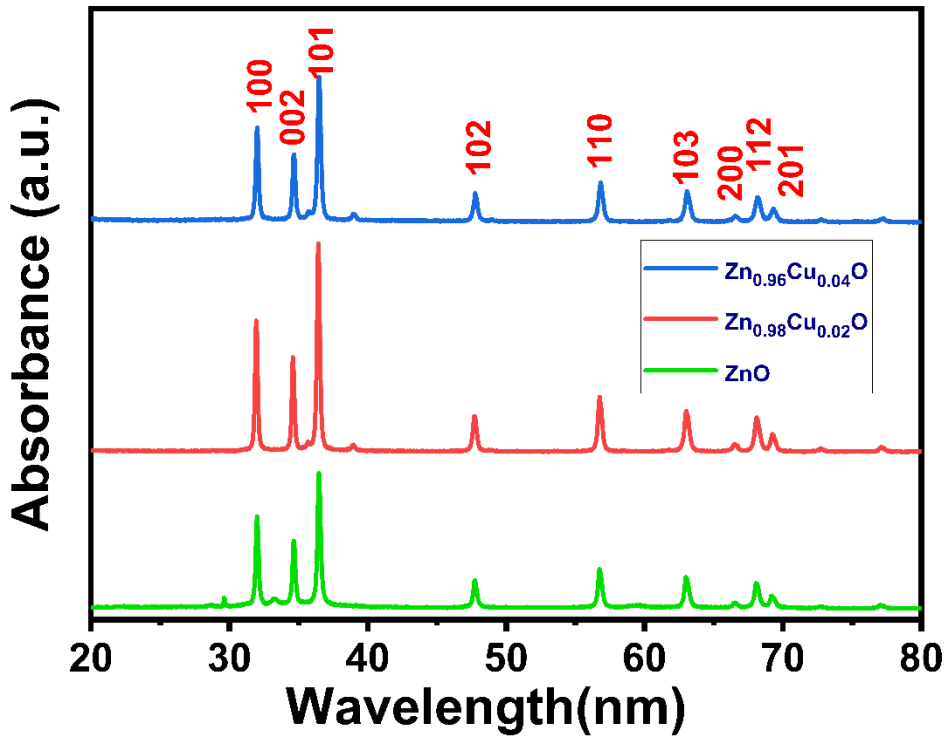

Figure 4. Comparison of the XRD pattern of all NPs: ZnO, $Zn_{0.98}Cu_{0.02}O$, and $Zn_{0.98}Cu_{0.02}O$

Debye-Scherer formula (Abu-Dief and Mohamed, 2017) was used to estimate the average grain size of crystallites (D_V) according to the following equations:

$$D_V = \frac{K\lambda}{\beta_{1/2}cos\theta} \quad (2)$$

Where K: 0.94 (for copper radiation), λ: 0.154056 nm, $\beta_{1/2}$: full width at half maximum (FWHM), θ: Bragg angle.

The induced microstrain (ε_m) was estimated by the equation:

$$\varepsilon_m = \frac{\beta_{1/2}cos\theta}{4} \quad (3)$$

For geometric structure, lattice parameters (LP) were determined using the following equation:

$$\frac{1}{d^2} = \frac{4}{3}\left(\frac{h^2+hk+l^2}{a^2}\right) + \frac{l^2}{c^2}$$

(4)

where h, k, and l are the Miller indices, a = b, c are the lattice constants, and d is the interplanar spacing. Interplanar spacing (d) was estimated using Bragg's law:

$$2dsin\theta = n\lambda$$

(5)

The dislocation density (δ_D) can be calculated by the following equation:

$$\delta_D = \frac{1}{D_V^2} \quad (6)$$

Table 1. XRD peak positions of different crystal planes

(hkl) planes 2θ	(100)	(002)	(101)	(102)	(110)	(103)	(200)	(112)	(201)
ZnO	31.762	34.424	36.250	47.542	56.601	62.882	66.611	67.972	69.115
$Zn_{0.98}Cu_{0.02}O$	31.685	34.358	36.182	47.483	56.538	62.815	66.473	67.905	69.035
$Zn_{0.96}Cu_{0.04}O$	31.670	34.340	36.163	47.460	56.113	62.790	66.443	67.875	69.006

After determining the lattice parameters a and c, it is possible to compute other structural parameters such as the volume of the unit cell (VUC), atomic packing fraction (APF), and bond length (BL) of Zn – O using Equations 7, 8, and 9, respectively.

$$VUC = 0.866a^2c \quad (7)$$

$$APF = \frac{2\pi a}{3\sqrt{3c}} \quad (8)$$

$$BL = \sqrt{\left(\frac{a^2}{3} + \left(\frac{1}{2} - u\right)^2 a^2 c\right)} \quad (9)$$

Where $u = \frac{a^2}{3c^2}$, and is commonly known as a positional parameter.

The results for different estimated structural parameters are displayed in Table 2. The nanoparticles' size increased from 38 to 42 nm as the copper content increased from 0 to 4% (Chithra et al., 2016). When Cu is added, the hexagonal wurtzite structure remains unchanged. However, as the concentration of Cu increases, the XRD peak position shifts towards a lower 2θ angle, suggesting that Cu has been introduced into the ZnO matrix. The shift in peak positions towards the lower 2θ angle may be a result of replacing Zn^{2+} (ionic radius of 0.74 Å) with Cu^{2+} (ionic radius of 0.73 Å) (Vegard , 2021). As the Cu concentration increases, the diffraction intensity increases, providing further evidence of Cu's presence in the ZnO structure. The calculated crystal defect parameters, such as the induced micro-strain and dislocation density, decreased with increased Cu concentration. The ZnO nanostructure has lattice constants a = 3.250 and c = 5.210 Å. The lattice constant was calculated as a = 3.250 Å and 5.307 Å for undoped ZnO. An increase in the lattice parameters "a" and "c" was observed on Cu doping. It is evident from the increase in lattice constants that the Cu ion has

been effectively incorporated into the ZnO matrix, possibly due to the substitution of Zn^{2+} with Cu^{+} and Cu^{2+} ions. As the concentration of Cu was increased from 0 to 4%, the VUC saw a significant increase of about 0.8%. The APF of each sample was determined to be 73.12%. The measured BL falls within the range of 1.988 and 1.992 Å.

Table 2. Different Structural parameters of $Zn_{1-x}Cu_xO$

Sample	Crystallite size (D_V)	Microstrain (ε_m)	Lattice constant (A^0)		Dislocation density ($\times10^{-4}$) (δ_D)	Unit cell volume $(A^0)^3$	APF (%)	BL (A^0)
ZnO	38.42	0.3432	3.341	5.367	7.35	50.23	73.12	1.988
$Zn_{0.98}Cu_{0.02}O$	41.46	0.3212	3.352	5.372	5.86	50.76	73.12	1.990
$Zn_{0.96}Cu_{0.04}O$	41.88	0.3285	3.361	5.378	5.94	50.82	73.12	1.992

3.3. Antibacterial activity and effect of Cu doping in ZnO NPs

The agar well diffusion technique evaluates the antibacterial potential of produced copper doped ZnO-NPs. In this investigation, two bacterial strains were used: Escherichia coli (E. coli), a gram-negative bacterium, and Streptococcus pyogenes, a gram-positive bacterium. Table 3 shows the diameter of inhibition zones (DOIZs) for all samples from selected gram-positive and gram-negative bacteria. It is interesting to observe that all bacterial pathogens were susceptible to the samples. However, gram-negative bacteria were more susceptible to the samples. This might be owing to the electrostatic attraction between positively charged Zn^{2+} and negatively charged cell wall lines of gram-negative bacteria. Furthermore, gram-positive bacteria have a thick coating of peptidoglycan (20-80 nm) in their cell walls, whereas gram-negative bacteria have a thin layer of peptidoglycan (2-3 nm) (Hajipour et al., 2012). As a result, the produced NPs interacted more readily with gram-negative bacteria. As the concentration of Cu-doped ZnO-NPs increases, so does the DOIZ. The increase in DOIZs seen with 2 and 4% Cu doping might be attributed to the Cu ion-induced redshift in the energy band gap of ZnO NPs and the observed particle aggregation. Figure 5 shows a clear difference in antibacterial activity between undoped and Cu-doped ZnO-NPs.

Table 3. ZOI (mm) of $Zn_{1-x}Cu_xO$ NPs against different bacteria

Serial No.	Sample	Diameter of inhabitation zone (mm)±standard error		Control (HCl)
		S. pyogenes (gram-positive)	*E. Coli* (gram-negative)	
1	ZnO	19±0.7	21±0.5	---
2	$Zn_{0.98}Cu_{0.02}O$	21±0.8	23±0.3	---
3	$Zn_{0.96}Cu_{0.04}O$	22±0.6	24±0.3	---

The antibacterial properties of ZnO may be attributed to factors such as the size of the nanoparticles (NPs), surface flaws, the release of Zn^{2+}, and the induction of oxidative stress. The typical diameter of a bacterium's cell wall is around 1 μm, which is almost 250 times larger than that of a ZnO NPs (Yousef and Danial, 2012). These nanoparticles have the ability to easily stick to and enter the cell walls of the bacterium, causing the microorganism to be destroyed and killed. The presence of surface flaws in ZnO nanoparticles allows for the interaction between ZnO nanoparticles and microorganisms, as a result of the presence of reactive sites. This interaction may take place in conjunction with the fundamental components of the outer cell membrane and has the potential to deteriorate or trigger structural alterations that might result in cell demise. The liberation of Zn^{2+} in the surrounding environment plays a crucial role in the harmful consequences of ZnO nanoparticles (Song et al., 2010). The released Zn^{2+} exerts bactericidal effects by interfering with the amino acid metabolism and enzymatic system of the microbe. Zinc and copper ions form crosslinks with nucleic acid strands through interactions with the microorganism's DNA. This leads to the denaturation of proteins and complete destruction of the bacterial cell. The oxidative stress mechanism may be attributed to the ability of ZnO nanoparticles (NPs) to generate reactive oxygen species (ROS), such as superoxide (O_2^-), hydroxyl (OH^-), and hydrogen peroxide (H_2O_2) radicals, on their surfaces through a photocatalytic process. Hydrogen peroxide radicals have the ability to penetrate the cell wall membrane of bacteria, leading to detrimental effects or even the death of the cell (Sirelkhatim et al., 2015).

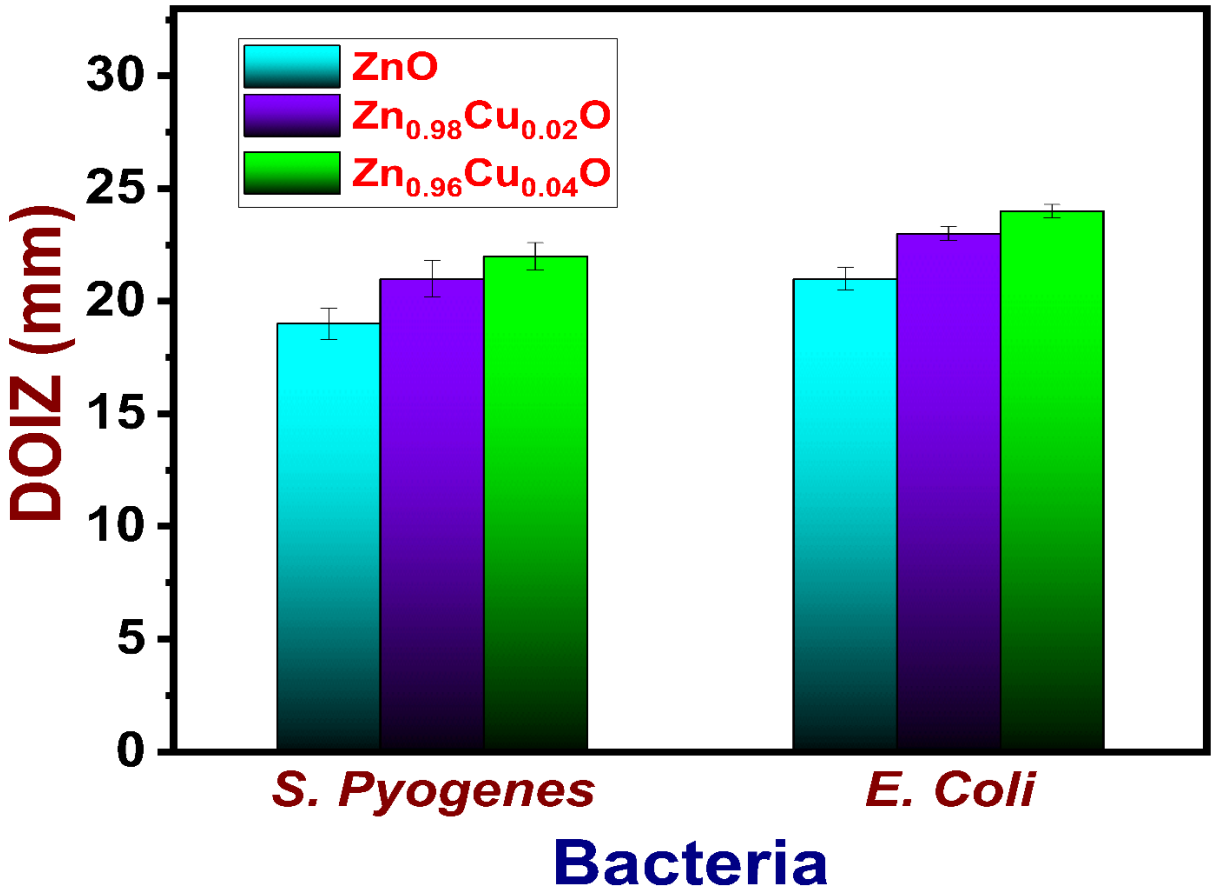

Figure 5. Bar graph showing the diameter of the zone of inhibition (in mm) produced by ZnO, $Zn_{0.98}Cu_{0.02}O$, and $Zn_{0.94}Cu_{0.04}O$ NPs against gram-positive and gram-negative bacteria.

4. Conclusions

The current research utilized Calotropis gigantea leaf extract to effectively synthesize copper-doped zinc oxide nanoparticles with concentrations of 0%, 2%, and 4%. The samples were thoroughly analyzed to examine their structural, morphological, and optical features using X-ray diffraction (XRD), scanning electron microscopy (SEM), and ultraviolet-visible (UV-Vis) spectroscopy. The samples exhibited a crystalline nature with a wurtzite hexagonal structure. The size of the crystallites grew from 38.42 to 41.88 nm when the Cu concentration rose from 0 to 4%. The Energy band gap decreased from 3.31 to 3.02 eV when the content of Cu increased from 0 to 4%. The antibacterial analysis revealed that the chosen pathogens exhibited susceptibility to the produced samples. Nevertheless, Cu-doped ZnO nanoparticles exhibited superior antibacterial properties against the selected pathogens.

Acknowledgment

The authors thank the Department of Physics, Bankura University, and Bankura Zilla Saradamani Mahila Mahavidyapith.

References

Ali, A., Ovais, M., Cui, X., Rui, Y., & Chen, C. (2020). Safety assessment of nanomaterials for antimicrobial applications. *Chemical Research in Toxicology*, **33(5),** 1082-1109.

Donlan, R. M. (2008). Biofilms on central venous catheters: is eradication possible? *Bacterial biofilms*, 133-161.

Okeke, I. S., Agwu, K. K., Ubachukwu, A. A., Maaza, M., & Ezema, F. I. (2020). Impact of Cu doping on ZnO nanoparticles phyto-chemically synthesized for improved antibacterial and photocatalytic activities. *Journal of Nanoparticle Research*, **22,** 1-18.

Wijesinghe, U., Thiripuranathar, G., Iqbal, H., & Menaa, F. (2021). Biomimetic synthesis, characterization, and evaluation of fluorescence resonance energy transfer, photoluminescence, and photocatalytic activity of zinc oxide nanoparticles. *Sustainability*, **13(4),** 2004.

Majumder, S., Chatterjee, S., Basnet, P., & Mukherjee, J. (2020). ZnO based nanomaterials for photocatalytic degradation of aqueous pharmaceutical waste solutions–A contemporary review. *Environmental Nanotechnology, Monitoring & Management*, **14**, 100386.

Hezam, A., Namratha, K., Drmosh, Q. A., Chandrashekar, B. N., Jayaprakash, G. K., Cheng, C., ... & Byrappa, K. (2018). Electronically semitransparent ZnO nanorods with superior electron transport ability for DSSCs and solar photocatalysis. *Ceramics International*, **44(6)**, 7202-7208.

Jhaveri, J., Raichura, Z., Khan, T., Momin, M., & Omri, A. (2021). Chitosan nanoparticles-insight into properties, functionalization and applications in drug delivery and theranostics. *Molecules*, **26(2)**, 272.

Zhang, W., He, H., Li, H., Duan, L., Zu, L., Zhai, Y., ... & Zhao, D. (2021). Visible-light responsive TiO2-based materials for efficient solar energy utilization. *Advanced Energy Materials*, **11(15)**, 2003303.

Samadi, M., Zirak, M., Naseri, A., Khorashadizade, E., & Moshfegh, A. Z. (2016). Recent progress on doped ZnO nanostructures for visible-light photocatalysis. *Thin Solid Films*, **605**, 2-19.

Gaurav, A., Beura, R., Kumar, J. S., & Thangadurai, P. (2019). Study on the effect of copper ion doping in zinc oxide nanomaterials for photocatalytic applications. *Materials Chemistry and Physics*, **230**, 162-171.

Shanmugam, V., & Jeyaperumal, K. S. (2018). Investigations of visible light driven Sn and Cu doped ZnO hybrid nanoparticles for photocatalytic performance and antibacterial activity. *Applied Surface Science*, **449**, 617-630.

Mintcheva, N., Aljulaih, A. A., Wunderlich, W., Kulinich, S. A., & Iwamori, S. (2018). Laser-ablated ZnO nanoparticles and their photocatalytic activity toward organic pollutants. *Materials*, **11(7)**, 1127.

Devi, P. G., & Velu, A. S. (2016). Synthesis, structural and optical properties of pure ZnO and Co doped ZnO nanoparticles prepared by the co-precipitation method. *Journal of Theoretical and Applied Physics*, **10(3)**, 233-240.

Al Abdullah, K., Awad, S., Zaraket, J., & Salame, C. (2017). Synthesis of ZnO nanopowders by using sol-gel and studying their structural and electrical properties at different temperature. *Energy Procedia*, **119**, 565-570.

Navidpour, A. H., Hosseinzadeh, A., Zhou, J. L., & Huang, Z. (2023). Progress in the application of surface engineering methods in immobilizing TiO2 and ZnO coatings for environmental photocatalysis. *Catalysis Reviews*, **65(3),** 822-873.

Jain, J., Arora, S., Rajwade, J. M., Omray, P., Khandelwal, S., & Paknikar, K. M. (2009). Silver nanoparticles in therapeutics: development of an antimicrobial gel formulation for topical use. *Molecular pharmaceutics*, **6(5),** 1388-1401.

Salem, S. S., & Fouda, A. (2021). Green synthesis of metallic nanoparticles and their prospective biotechnological applications: an overview. *Biological trace element research*, **199(1),** 344-370.

Mohamad, N. A. N., Arham, N. A., Jai, J., & Hadi, A. (2014). Plant extract as reducing agent in synthesis of metallic nanoparticles: a review. *Advanced Materials Research*, **832,** 350-355.

Berehu, H. M., S, A., Khan, M. I., Chakraborty, R., Lavudi, K., Penchalaneni, J., ... & Patnaik, S. (2021). Cytotoxic potential of biogenic zinc oxide nanoparticles synthesized from swertia chirayita leaf extract on colorectal cancer cells. *Frontiers in bioengineering and biotechnology*, **9,** 788527.

Ahmed, S., Chaudhry, S. A., & Ikram, S. (2017). A review on biogenic synthesis of ZnO nanoparticles using plant extracts and microbes: a prospect towards green chemistry. *Journal of Photochemistry and Photobiology B: Biology*, **166,** 272-284.

Karale, P. A., & Karale, M. A. (2017). A review on phytochemistry and pharmacological properties of milkweed family herbs (Asclepiadaceae). *Asian J Pharm Clin Res*, **10(11),** 27-34.

Wiegand, I., Hilpert, K., & Hancock, R. E. (2008). Agar and broth dilution methods to determine the minimal inhibitory concentration (MIC) of antimicrobial substances. *Nature protocols*, **3(2),** 163-175.

Tauc, J., Grigorovici, R., & Vancu, A. (1966). Optical properties and electronic structure of amorphous germanium. *physica status solidi (b)*, **15(2),** 627-637.

Guneri, E., Ulutas, C., Kirmizigul, F., Altindemir, G., Gode, F., & Gumus, C. (2010). Effect of deposition time on structural, electrical, and optical properties of SnS thin films deposited by chemical bath deposition. *Applied Surface Science*, **257(4),** 1189-1195.

Bylsma, R. B., Becker, W. M., Kossut, J., Debska, U., & Yoder-Short, D. (1986). Dependence of energy gap on x and T in Zn 1− x Mn x Se: the role of exchange interaction. *Physical Review B*, **33(12),** 8207.

Liang, Q., Qiao, F., Cui, X., & Hou, X. (2019). Controlling the morphology of ZnO structures via low temperature hydrothermal method and their optoelectronic application. *Materials Science in Semiconductor Processing*, **89,** 154-160.

Abu-Dief, A. M., & Mohamed, W. S. (2017). α-Bi2O3 nanorods: synthesis, characterization and UV-photocatalytic activity. *Materials Research Express*, **4(3),** 035039.

Chithra, M. J., & Pushpanathan, K. (2016). Thermal, structural and optical investigation of Cu-doped ZnO nanoparticles. *Modern Physics Letters B*, **30(34),** 1650406.

Vegard, L. (1921). IV. Recent results of northlight investigations and the nature of the cosmic electric rays. *The London, Edinburgh, and Dublin Philosophical Magazine and Journal of Science*, **42(247),** 47-87.

Hajipour, M. J., Fromm, K. M., Ashkarran, A. A., de Aberasturi, D. J., de Larramendi, I. R., Rojo, T., ... & Mahmoudi, M. (2012). Antibacterial properties of nanoparticles. *Trends in biotechnology*, **30(10),** 499-511.

Yousef, J. M., & Danial, E. N. (2012). In vitro antibacterial activity and minimum inhibitory concentration of zinc oxide and nano-particle zinc oxide against pathogenic strains. *J Health Sci*, **2(4),** 38-42.

Song, C., Qu, Z., Blumm, N., & Barabási, A. L. (2010). Limits of predictability in human mobility. *Science*, *327*(5968), 1018-1021.

Sirelkhatim, A., Mahmud, S., Seeni, A., Kaus, N. H. M., Ann, L. C., Bakhori, S. K. M., ... & Mohamad, D. (2015). Review on zinc oxide nanoparticles: antibacterial activity and toxicity mechanism. *Nano-micro letters*, **7,** 219-242.